Equilibrium sampling of self-associating polymer solutions: A parallel selective tempering approach

Chakravarthy Ayyagari,[a] Dmitry Bedrov, and Grant D. Smith
Department of Chemical and Fuels Engineering and Department of Materials Science and Engineering,
University of Utah, 122 S. Central Campus Drive, Room 304, Salt Lake City, Utah 84102

We present a novel simulation algorithm based on tempering a fraction of relaxation-limiting interactions to accelerate the process of obtaining uncorrelated equilibrium configurations of self-associating polymer solutions. This approach consists of tempering (turning off) the attractive interactions for a fraction of self-associating groups determined by a biasing field h. A number of independent configurations (replicas) with overlapping Hamiltonian distributions in the expanded ($NVTh$) ensemble with constant NVT but different biasing fields, forming a chain of Hamiltonians, were simulated in parallel with occasional attempts to exchange the replicas associated with adjacent fields. Each field had an associated distribution of tempered interactions, average fraction of tempered interactions, and structural decorrelation time. Tempering parameters (number of replicas, fields, and exchange frequencies) were chosen to obtain the highest efficiency in sampling equilibrium configurations of a self-association polymer solution based on short serial simulation runs and a statistical model. Depending on the strength of the relaxation-limiting interactions, system size, and thermodynamic conditions, the algorithm can be orders of magnitude more efficient than conventional canonical simulation and is superior to conventional temperature parallel tempering. © 2005 American Institute of Physics. [DOI: 10.1063/1.1979494]

I. INTRODUCTION

In simulations of self-associating systems structural heterogeneity can add tremendous complexity to sampling configurational space. Such systems often have complex energy landscapes with disconnected low-energy states allowing configurations to become trapped in local minima. For self-associating molecular systems (e.g., surfactants, ionomers, and block copolymers) this corresponds to the formation of energetically stable domains (e.g., clusters, micelles, multiplets, or microphases). In order for structural relaxation and sampling of uncorrelated equilibrium configurations, molecules must make a transition from one energetically stable domain to another, typically requiring the molecules to visit high-energy states. The greater the barrier for transitioning between two local minima relative to the thermal energy the larger the bottleneck this process is to structural relaxation in the system. Similar issues have been noticed earlier in dense polymer melts, spin glasses, and supercooled liquids. Generating uncorrelated equilibrium configurations of such systems with conventional simulation methods is a formidable task. In recent years, several algorithms have been developed to overcome this problem. Some of the methodologies that were employed are multicanonical sampling,[1,2] 1/k sampling,[3] J walking,[4,5] expanded ensembles,[6] simple tempering,[7,8] entropic tempering,[9] parallel tempering,[10–13] hyper-parallel tempering,[14] and replica exchange (Monte Carlo[15] and molecular dynamics[16,17]). These techniques have been applied in simulating complex systems such as peptides,[11,12,18] dense polymer melts,[19] spin glasses,[20] lattice

quantum chromodynamics (QCD),[21,22] supercooled liquids as well as simple models like two-dimensional (2D) spin[23] and Lennard-Jones[24] fluids. Various studies using these methods have elucidated phase behavior in Lennard-Jones clusters[25,26] and water octamers,[27] thermodynamics of Ar_n−HF clusters,[28,29] conformational studies of polymer melts,[30] and reconstruction of porous media.[31]

Parallel-tempering methods typically involve coupling independent replicas (realizations of the same physical system) simulated at slightly different conditions, controlled by either one or more variables. The controlling parameter can be temperature, as in temperature parallel tempering, chemical potential as in hyperparallel tempering, a delocalization parameter, as in the q-jumping Monte Carlo[32] method or any other suitable parameter that modifies the Hamiltonian thereby forming a chain of Hamiltonians. Neighboring replicas along the chain are occasionally swapped to allow each replica to visit different conditions, thus allowing each replica to explore the phase space associated with each Hamiltonian. To apply parallel tempering successfully the phase-space densities associated with adjacent Hamiltonians along the chain must have sufficient overlap. Moreover, this overlap of phase space between any two neighboring Hamiltonians (and their current replicas) must ensure that the switching of replicas leads to a random walk of each replica in the extended variable space, i.e., along the chain of Hamiltonians. To guarantee an efficient random walk the probability of its switching with neighboring replicas must be symmetric and constant along the entire chain.

The efficiency of the parallel tempering algorithm will depend on the number of replicas employed and the manner

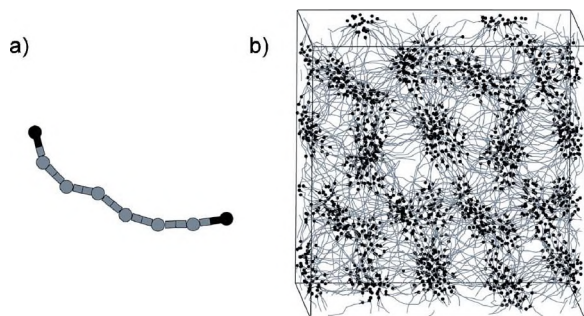[a] Electronic mail: chak@eng.utah.edu

FIG. 1. (a) A single telechelic chain with eight-beads. Attractive beads are represented by black. (b) Formation of clusters in a canonical ensemble of 1000 chains at $T=0.1$.

in which the replicas are spaced in configuration space. In the case of temperature parallel tempering, one of the simplest to implement and most commonly employed variation of the parallel tempering, distributions of potential energies are considered for swapping the configurations. As the system size increases, the width of the distribution of energies (or any other appropriate conjugate property to the controlling parameter) compared to its average value becomes narrower and the number of replicas required to provide equivalent overlapping of phase space will be larger. Predescu et al.[33] have determined that the efficiency of temperature parallel tempering Monte Carlo method for classical canonical systems decreases naturally to zero with increasing system size.

Here we describe a novel parallel selective tempering (PST) algorithm based on earlier realization of expanded ensemble simulations of dense systems.[34] Unlike the conventional parallel tempering techniques where all interactions in the system are tempered simultaneously, we target specific interactions that are responsible for slow structural relaxation and temper only a fraction of these interactions. In case of self-assembling polymer solutions it is obvious that the relaxation of the entire structure is controlled by interactions responsible for self-association of the polymer chains. We also investigate the effect of the parameters of the parallel tempering algorithm such as the number of replicas and acceptance probability for replica exchanges on the efficiency of the algorithm. Optimal parameters were chosen by systematic investigation involving performing model PST runs using a statistical model presented in this paper. This model requires only input provided by short serial simulation runs performed in $NVTh$ ensemble at different values of the controlling parameter h. The efficiency of the PST algorithm was compared to temperature parallel tempering (TPT). We also investigate the efficiency of the PST method as a function of system size and temperature.

II. MOLECULAR-DYNAMICS SIMULATIONS OF SELF-ASSOCIATING POLYMER SOLUTIONS

A. Simulation methodology and system description

Simulations were performed on an ensemble of 1000 telechelic chains of eight beads each where chain ends are designated as "stickers." A pictorial representation of the system is illustrated in Fig. 1. This system is identical to the

telechelic solutions studied in our previous work.[35,36] Note that the potential used in this previous work is identical to that given here, and not as published in that work. This form of the potential was originally used in the work of Khalatur et al.[37] In our simulations all beads interact via a simple Weeks-Chandler-Andersen (WCA) potential (purely repulsive) given by,

$$U(r) = \begin{cases} 4\left(\dfrac{\varepsilon}{9}\right)\left[(\sigma/r)^{12} - (\sigma/r)^{6} + \dfrac{1}{4}\right], & r < r_0 \\ 0, & r \geq r_0, \end{cases} \quad (1)$$

where $r_0 = 2^{1/6}$. This potential represents the excluded volume interactions between any two nonbonded particles and is a good model for a polymer chain immersed in a good solvent. In addition to the WCA interaction, the end-groups (stickers) interact via a screened attractive Coulomb potential of the form:

$$U_c(r) = \begin{cases} -\dfrac{\varepsilon}{r}[1 - (r/r_c)^2]^2, & r < r_c \\ 0, & r \geq r_c, \end{cases} \quad (2)$$

with a screening length $r_c = 2$. Bond lengths were constrained at unit length by employing the SHAKE algorithm.[38] Additional rigidity was introduced by a bend potential of the form

$$U_b(r) = k_b(A - A_0)^2, \quad (3)$$

where $k_b = 0.593$ and the equilibrium bend angle (A_0) of 175°. All properties described in this paper are expressed in reduced units,[39] in terms of the energy scale ε, length scale σ, and bead mass m, specifically time ($t = [\varepsilon/(m\sigma^2)]^{1/2}t^*$), density ($\rho = \rho^*\sigma^3$), temperature ($T = k_B T^*/\varepsilon$), and frequency ($\omega = [\varepsilon/(m\sigma^2)]^{-1/2}\omega^*$).

Molecular-dynamics (MD) simulations were performed at various temperatures (0.1–0.74) with a constant density (0.3) and NVT conditions. A Nose-Hoover[40,41] thermostat with a thermostat frequency of 2.5 was employed to regulate temperature in all our simulations. Initially, the molecules were placed on a low-density lattice. Simulations were carried out in NPT ensemble for 1×10^6 steps at high temperature (0.37) with a reduced time step of 0.01. Later, NVT simulations were performed at $T=0.37$ at equilibrium density obtained from NPT simulations. The system underwent several hundred relaxation times (calculated from the chain end-end vector autocorrelation function) during the length of the simulation. Subsequently the systems were cooled over another 1×10^6 steps to desired temperatures at a constant density (0.3). Equilibration runs were performed for at least two relaxation times at lower temperatures and several relaxation times at high temperatures except for $T=0.1$ where the relaxation time is about 2×10^6 (2×10^8 time steps). Subsequently, production runs were carried out for several relaxation times at each temperature except for $T=0.1$ and statistics were collected to obtain equilibrium properties.

B. Structure and structural relaxation

Stickers tend to self-associate to form clusters (as seen in Fig. 1), the size, shape, distribution, and spacing of which is dependent on the thermodynamic conditions. For example,
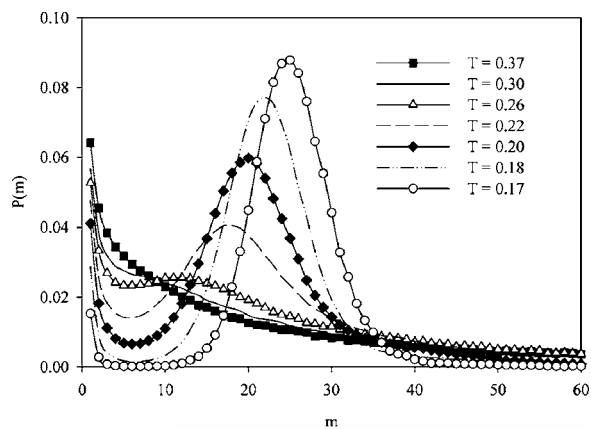
FIG. 2. Probability to find an end group in a cluster of size m for self-associating polymer solutions as a function of temperature.

the cluster size distribution, defined as the probability $P(m)$ to find an end group in a cluster of size m, is shown as a function of temperature in Fig. 2. Here a cluster of size m is defined as an aggregation of end-groups in which each chain end group is within a distance of 2 from at least one other end group in the cluster. Similar to our earlier simulations of self-associating polymer solutions we observe an onset of micellization (appearance of a shoulder in cluster size distribution) at around $T=0.26$, or T_m, below which end-groups aggregate to form clusters of preferable size.

Also consistent with our previous studies we discern that the formation of clusters strongly influences the dynamical properties and viscoelastic response of the polymer solution. The terminal relaxation time as a function of temperature, obtained by fitting the chain end-to-end vector autocorrelation function obtained from MD simulations with a stretched exponential and integrating over time,

$$\tau_{\text{terminal}} = \int C(t)dt = \int \exp[-(t/\tau)^\beta]dt \qquad (4)$$

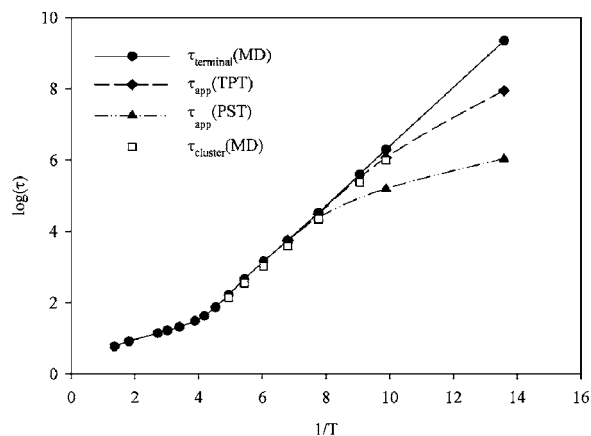is shown in Fig. 3. The relaxation times in the self-associating regime $(T<T_m)$ show an Arrhenius dependence

FIG. 3. Temperature dependence of terminal relaxation times (τ_{terminal}) and cluster life times (τ_{cluster}) of self-associating solutions obtained from MD simulations. Also shown are the apparent relaxation times (τ_{app}) resulting from parallel selective tempering (PST) and temperature parallel tempering (TPT) algorithms.

on temperature with an apparent activation energy that is significantly higher than that observed for $T>T_m$. The relaxation time at $T=0.07$ was extrapolated based on Arrhenius behavior at higher temperatures. Structural relaxation in the self-associating polymer solution was monitored through the cluster lifetime autocorrelation function, defined as

$$ACF_{\text{cluster}} = \frac{\sum_{i \neq j} H_{ij}(t) \cdot H_{ij}(0)}{\sum_{i \neq j} H_{ij}(0) \cdot H_{ij}(0)}, \qquad (5)$$

where the summation was performed over every pair (i,j) of end groups. Here the function $H_{ij}(t)=1$ if the end groups i and j belong to the same cluster at time t, otherwise $H_{ij}(t)=0$. The cluster lifetime (τ_{cluster}) was obtained by fitting Eq. (5) to a stretched exponential and integrating over time [see Eq. (4)]. As in our previous studies we can see in Fig. 3 a close correspondence between the cluster lifetime and the end-to-end vector relaxation time of the telechelic chains.

An important consequence of the dramatic increase in the terminal relaxation time of the telechelic chains with decreasing temperature resulting from the formation of stable end-group clusters for $(T<T_m)$ is that obtaining equilibrium configurations using conventional MD simulations quickly becomes infeasible with decreasing temperature. To enhance the structural decorrelation process in these self-associating polymer solutions a parallel selective tempering methodology described in Sec. III has been employed.

III. THE PARALLEL SELECTIVE TEMPERING (PST) METHOD

A. Ghost particles

Our supposition is that obtaining the equilibrium configuration of a molecular system can be greatly facilitated by tempering a subset of interactions that is responsible for the slowing down of dynamics if these interactions are known *a priori*. In case of the self-associating polymer solution described in Sec. II, structural relaxation is limited by the ability of self-associating groups to leave a cluster and join other clusters, a process that can be monitored through relaxation of the polymer chain end-to-end vector autocorrelation function. To facilitate relaxation, the attraction leading to formation of these energetically stable clusters (relaxation-limiting interactions) can be either reduced (by a scaling factor) or completely eliminated. In either case self-associating particles are allowed to move into a nonphysical space in which their interaction with other particles has been modified. Each "allowable" particle i is assigned a fictitious space coordinate depending on the current interaction state. A value of "0" for this coordinate, $x_4(i)=0$, indicates that all interactions due to this particle are included whereas $x_4(i)=1$ represents a particle whose interactions are modified. A system that has all particles with the fourth coordinate as 0, $\vec{x}_4=0$, represents the unperturbed system. The extended Hamiltonian for this system is given by

$$H(\vec{x}, \vec{x}_4) = U(\vec{x}, \vec{x}_4). \qquad (6)$$

The potential energy depends not only on the real space coordinates of all particles, given by $\vec{x}$, but also on $\vec{x}_4$, as par-

ticles with $x_4(i) = 1$ have modified interactions with the remaining particles.

The number of allowable particles is fixed and is specific to the system under study. For example, in the case of self-associating polymer solutions, we have chosen only the sticky groups (with mutually attractive potentials) to be allowable particles. The probability of transition of a particle from $x_4(i) = 0$ to $x_4(i) = 1$ and vice versa is subject to the Metropolis criterion given by:

$$P(x_4(i) = 0 \Leftrightarrow x_4(i) = 1) = \begin{cases} 1, & \Delta H \leq 0 \\ \exp(-\beta \Delta H), & \Delta H > 0, \end{cases}$$

(7)

where ΔH is the change in the Hamiltonian [Eq. (6)] associated with the (attempted) transition β is $1/k_B T$. In our study, a particle with $x_4(i) = 1$ has no nonbonded interactions with any other particles. Hence these particles will be referred to as "ghost" particles throughout the rest of the paper. Note, however, that the bonded interactions (bond and bend) involving these particles are unaffected by this transition.

B. Extended Hamiltonian and external biasing field

The equilibrium number of ghost particles obtained in a system with a Hamiltonian given by Eq. (6) can be controlled by applying a biasing field h that operates only on particles with $x_4(i) = 1$. The associated Hamiltonian is

$$H(h, \vec{x}, \vec{x}_4) = U(\vec{x}, \vec{x}_4) + N_{\text{allowable}} f_4 h,$$

(8)

where $N_{\text{allowable}}$ is the number of allowable particles and f_4 is the fraction of allowable particles with $x_4(i) = 1$. The associated partition function for the $NVTh$ ensemble is

$$\Pi(NVTh) = \sum_{\vec{x}} \sum_{\vec{x}_4}$$

$$\times \exp[-\beta U(\vec{x}, \vec{x}_4)] \exp[-\beta N_{\text{allowable}} f_4 h].$$ (9)

It can be straightforwardly shown[42] that in the $NVTh$ ensemble the fluctuations in f_4 are given as

$$\sigma_{f_4}(h) = \chi^{1/2} N_{\text{allowable}}^{-1/2},$$

(10)

where the field susceptibility is given by

$$\chi = -\frac{1}{\beta} \frac{\partial \bar{f}_4}{\partial h},$$

(11)

and $\bar{f}_4$ is the ensemble average of f_4.

From Eq. (8) we can conclude that an increase in the field will penalize particles with $x_4(i) = 1$ and hence will result in a decrease in $\bar{f}_4$. Conversely, a decrease in the field will favor particles with $x_4(i) = 1$ and will result in an increase in $\bar{f}_4$. The important point to realize is that for a given system and given thermodynamic conditions the average value of the fraction of ghost particles $\bar{f}_4$ is determined by the field once equilibrium is reached. Furthermore, Eq. (10) reveals that during a simulation in the $NVTh$ ensemble (see Sec. III D for simulation details) f_4 fluctuates with time around the mean value and the identity of particles that con-
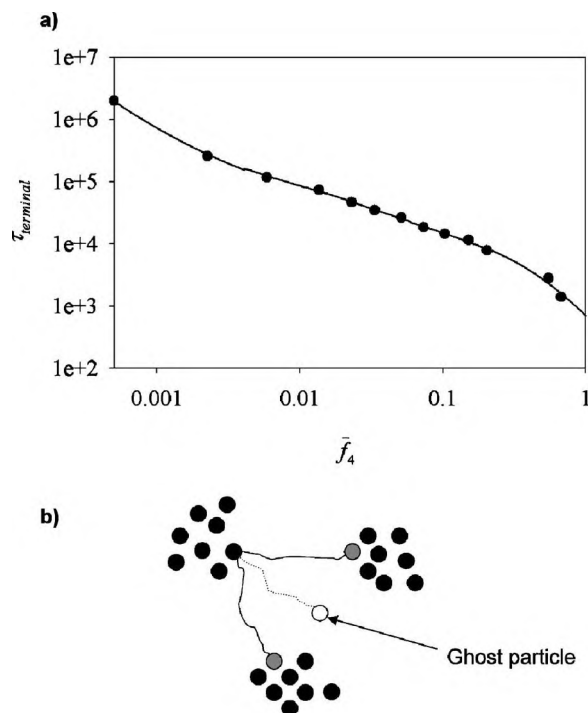

FIG. 4. (a) Terminal relaxation times (τ_{terminal}) obtained from serial $NVTh$ simulations as a function of average fraction of ghost particles ($\bar{f}_4$) at $T = 0.1$. (b) Schematic illustration of "cluster hopping" mechanism.

tribute to f_4 vary with time. Eventually, all allowable particles (should) participate in transition from real to ghost (nonphysical) space and vice versa.

C. Role of ghost particles on relaxation dynamics

We have found that the structural relaxation in the micelle-forming polymer solution described in Sec. II B is closely related to the end-to-end vector relaxation of individual chains. In other words, end-group clusters breakup and reform on the same time scale as the terminal relaxation of individual chains. The terminal relaxation time τ_{terminal} obtained by fitting the chain end-to-end vector autocorrelation function to a stretched exponential and integrating over time [see Eq. (4)] is shown as a function of $\bar{f}_4$ at $T = 0.1$ in Fig. 4(a). There is a significant reduction in the chain relaxation time as the average fraction of ghost particles increases, which in turn can be controlled by the strength of the applied field h.

We investigated the mechanism underlying the dramatic reduction in chain relaxation times as $\bar{f}_4$ increases for these self-associating polymer solutions. The chain ends with mutual attraction aggregate to form clusters. As a chain end group (allowable particle) moves from real space to ghost space, $x_4(i) = 0 \rightarrow x_4(i) = 1$, it no longer is bound to any cluster and is free to traverse the interstitial regions between the clusters. At a later time, as the ghost particle makes a transition back to the real space, $x_4(i) = 1 \rightarrow x_4(i) = 0$, it is likely to join a different cluster. For example, at $\bar{f}_4 = 0.001$ and $T = 0.1$, we observe that 85% of the time when a ghost particle is changed to a real particle it joins a cluster that is a different cluster than it was in before it transitioned into a ghost
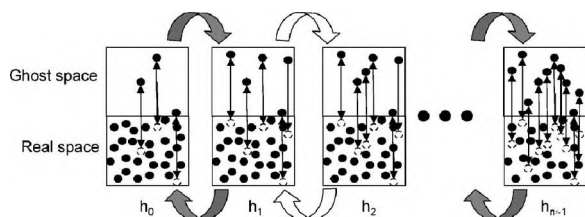
FIG. 5. Schematic illustration of parallel selective tempering (PST). Application of field h drives particles from real space to ghost space. Different shadings in double-sided block arrows indicate swapping at different times.

particle. This cluster-hopping mechanism [see Fig. 4(b)] seems to play the dominant role in the decrease of chain decorrelation times and increased efficiency in structural decorrelation as $\bar{f}_4$ increases.

D. Parallel selective tempering scheme

A parallel tempering technique utilizing the Hamiltonian given in Eq. (8) has been devised where n_r independent replicas (physical realizations) of a system are simulated in parallel. Each replica was simulated at a particular external field $(h_0 > h_1 > h_2 > h_i > \cdots > h_{n_r-1})$. Values of the external fields are chosen such that $\bar{f}_4$ increases monotonically with field index i. Moreover, each field is associated with a chain relaxation time τ_{terminal} that depends on $\bar{f}_4$.

1. Replica exchanges

Configurations between neighboring fields are swapped at regular intervals with a probability determined by the following Metropolis rule,

$$P(h_i \Leftrightarrow h_{i+1}) = \begin{cases} 1, & \Delta H \leqslant 0 \\ \exp(-\beta\Delta H), & \Delta H > 0, \end{cases} \quad (12)$$

where $\Delta H = -N_{\text{allowable}}\Delta f_4 \Delta h$, $\Delta f_4 = f_4^{i+1} - f_4^i$, f_4^{i+1} is the instantaneous value of f_4 for the replica experiencing field h_{i+1} at the time of the switching, f_4^i is the instantaneous value of f_4 for the replica experiencing field h_i and $\Delta h = h_{i+1} - h_i$. After every successful exchange, the replica previously experiencing field i is simulated under external field h_{i+1} and replica previously with field h_{i+1} is simulated under field h_i. Exchange of configurations at any particular instant are attempted in an alternate fashion with $i=1,3,5,\ldots$, or $i=2,4,6,\ldots$. Pictorial representation of the replica exchange scheme is illustrated in Fig. 5.

2. Particle moves

At each field, the coordinates in real space $(\vec{x})$ were updated utilizing MD simulations in the $NVTh$ ensemble with a Hamiltonian given by $U(\vec{x},\vec{x}_4)$ utilizing a time step of 0.01. After updating the real coordinates, a particle was selected randomly from the allowable particles (see Sec. III A) and a Monte Carlo move for update of its extended coordinate $x_4(i)$ was performed at each time step. Specifically, particles move from ghost space to real space and vice versa subject to criteria established by Eq. (7) with $\Delta H = \Delta U + \Delta n_i h_i$, where $\Delta n_i = 1$ for $x_4(i)=0 \rightarrow x_4(i)=1$ and $\Delta n_i = -1$ for $x_4(i)=1 \rightarrow x_4(i)=0$.
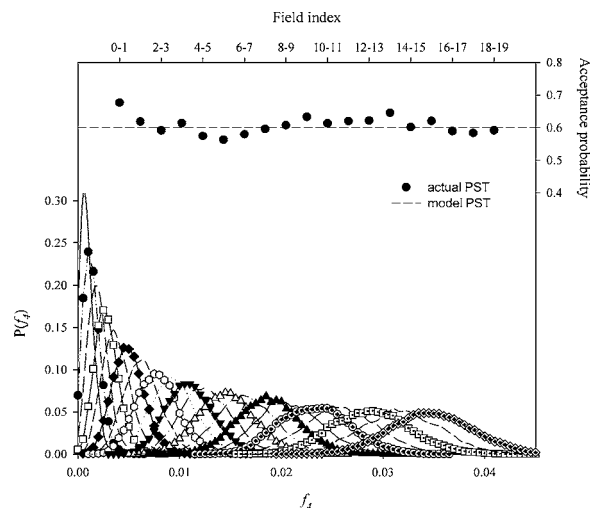

FIG. 6. Probability distributions of f_4 and the corresponding acceptance probability obtained from actual PST simulations using 20 replicas at $T=0.1$ and $\omega=0.008$. Desired probability (0.6) is shown by dotted line.

E. Algorithmic parameters

During PST, each replica (in principle) spends time at each field. The extent of chain (and structural) decorrelation for each replica depends upon the amount of time spent by that replica at each field, since the chain (and hence structural) relaxation time τ_{terminal} decrease as $\bar{f}_4$ increases, as shown in Fig. 4(a). However, each replica contributes structural data (statistics) only while residing in the first external field (h_0) whose corresponding equilibrium structure closely resembles that of the unperturbed system, i.e., has zero or so few ghost particles that they do not significantly perturb the structure (i.e., cluster size distribution) of the system. Optimization consists of determining the number of replicas, their associated fields, the exchange frequency between replicas and the frequency of attempted particle moves that allows uncorrelated equilibrium configurations to be produced and sampled at h_0 as efficiently as possible.

1. External fields

The probability of success in swapping neighboring replicas, and hence the rate at which replicas can migrate up and down the chain of fields, will be determined by the extent of overlap in the distributions of the value of the extended Hamiltonian [Eq. (8)] between neighboring fields. If each replica is simulated in a $NVTh$ ensemble under the same thermodynamic conditions (total number of particles, temperature and density), the swapping probability is given by Eq. (12) and the relevant distribution is the fraction of ghost particles f_4 at any particular field. As an example, Fig. 6 shows the distribution of f_4 for a chain of fields for a PST configuration for our telechelic system (see Sec. II) at $T=0.1$ comprised of 20 replicas. Also shown is the replica exchange acceptance probability corresponding to these overlaps (see Sec. VI). It is clear that the significant overlap in the distributions for neighboring replicas is required to obtain reasonable exchange acceptance probability.

The choice of starting field h_0 depends upon the effect of ghost particles on the structure of the system. Ideally, one has

to choose this parameter in a manner that simulations at this field provide configurations that resemble the unperturbed system (with no ghost particles). However, it is possible to consider h_0 such that $f_4(h_0) \neq 0$ but small enough that structure is unperturbed thereby "shortening" the length of the chain of fields required to reach a high $\bar{f}_4$ and hence fast structural decorrelation. Note also that the width of the distribution in f_4 decreases dramatically as $\bar{f}_4 \to 0$ (see Fig. 6) due to entropic reasons. Similarly, the width of the distribution in f_4 decreases as $\bar{f}_4 \to 1$ (not shown in the figure). Access to these regions of phase space requires closely spaced fields to obtain sufficient overlap (exchange probability) and is best avoided if possible. By performing the sensitivity analysis of ghost particles on structure, one can fix the starting field at a value that provides minimal tempering of the structure.

In order for a replica to perform a random walk through the chain of fields it is necessary to have uniform acceptance probability between any two adjacent replicas. The efficiency of the algorithm depends upon the choice of the acceptance rate, which is determined by the overlap in the distribution of $\bar{f}_4$ between neighboring fields (see Fig. 6), as well as in the acceptance rate being as constant as possible. A significantly lower acceptance rate between any two particular replicas results in a bottleneck that adversely affects the efficiency of the method. Hence, the fields h_i must be chosen to provide a constant acceptance rate for exchanges along the entire chain of fields.

2. Number of replicas (n_r)

Increasing the number of independent replicas, i.e., the length of the chain of fields, allows the maximum $\bar{f}_4$ to be increased for fixed replica exchange acceptance probability. However, as the length of the chain (number of replicas) increases at a constant acceptance probability, each replica in the chain requires more time to traverse (via a random walk) the entire chain of fields. Additionally, as mentioned above, access to very large $\bar{f}_4$ requires closely spaced fields. Therefore there will be a finite number of replicas that gives an optimal efficiency of the algorithm that must be determined.

3. Replica exchange attempt frequency (ω)

Once the exchange of replicas is successful, the replicas are simulated at new values of the biasing field. To reduce unwanted back jump correlations, the replicas are allowed to equilibrate to their new fields before another attempt of exchange is made. If the attempt is made soon after a successful exchange, thereby not allowing replicas to sample different energy space, the success of a consecutive attempt will be high. Therefore, at high frequencies, the neighboring configurations jump back and forth between two adjacent fields, forcing the replicas to sample the same phase space and thus reducing the efficiency of the algorithm. Even though a significant overlap in phase space (overlap in distribution in $\bar{f}_4$, see Fig. 6) is essential for a finite value of acceptance probability, the success of the algorithm depends on a uniform random walk of replicas through the chain of fields. Thus, if the frequency is too low, the diffusion of replicas in the chain of fields is reduced, thereby decreasing the efficiency of the PST algorithm. Thus, the replica exchange attempt frequency needs to be optimized for a particular system and the thermodynamic conditions at which the system is simulated.

4. Attempted particle moves

As mentioned in Sec. III D, the coordinates of particles in real space, $\vec{x}$, were updated via MD simulations and the extended fourth coordinate $\vec{x}_4$ was updated using Monte Carlo (MC) move. The MD simulation time step was chosen in such a way that the system traverses the phase space as fast as possible with minimal errors due to integration. The choice of frequency of MC moves must ensure a fast equilibration of number of ghost particles at any particular field h_i. Therefore, a reasonable choice would be attempting a MC move at each MD simulation time step on a particle selected randomly from the pool of allowable particles. Additionally, at every MD simulation time step, the MC attempts can be performed on multiple particles sequentially allowing the f_4 to reach the equilibrium value for a particular field.

IV. STATISTICAL MODEL

It is extremely difficult to empirically optimize the tempering parameters described above based on actual parallel tempering simulations. Therefore, we have developed a statistical model utilizing input from short serial simulations (no replica exchanges) performed over a wide range of fields that allows us to optimize the tempering parameters that can be subsequently utilized in actual PST runs (see Sec. VI).

A. Input parameters

At a given field strength h the fraction of ghost particles fluctuates around an equilibrium average value determined by the strength of the field, as discussed in Sec. III B. The distribution of the fraction of ghost particles f_4, like any other thermodynamic quantity, can be fit to a Gaussian. The width of the distribution σ_{f_4} depends on the size of the system, temperature, and strength of the field [see Eq. (10)]. Keeping the temperature and the size of the system constant, the mean value and the width of the distribution will be a function of strength of the field alone, as shown in Sec. III B. Also, as mentioned earlier in Sec. III E, the structural relaxation time τ_{terminal} depends on $\bar{f}_4$ which in turn depends upon the strength of the biasing field. Therefore,

$$\bar{f}_4 = \bar{f}_4(h, T),$$

$$\sigma_{f_4} = \sigma_{f_4}(\bar{f}_4, N_{\text{allowable}}, T) = \chi^{1/2}(\bar{f}_4, T) N_{\text{allowable}}^{-1/2},$$

$$\tau_{\text{terminal}} = \tau_{\text{terminal}}(\bar{f}_4, T). \tag{13}$$

Note that $N_{\text{allowable}}$ (in our case all end-groups) is proportional to the total number of particles in the system and hence is a measure of system size. Short serial simulations (without replica exchange) in $NVTh$ ensemble can be performed at constant $N_{\text{allowable}}$ and T to obtain $\bar{f}_4(h)$, $\sigma_{f_4}(\bar{f}_4)$,

and $\tau_{\text{terminal}}(\overline{f}_4)$ for discrete values of h. The characteristic values $(\overline{f}_4, \sigma_{f_4},$ and $\tau_{\text{terminal}})$ at any field can be obtained by interpolating from the values obtained from short serial simulations at discrete fields in $NVTh$ ensemble.

B. Random number generator

If σ_{f_4} and $\overline{f}_4$ at any particular field h are known, the distribution in f_4 can be modeled by employing the Gaussian random number generator. The Gaussian random number generator is easily obtained by employing Box-Muller[43] algorithm to the uniform random number (that gives a distribution of random numbers from 0 to 1). The distribution of Gaussian random numbers thus obtained will have a mean value of 0 and a width of 1. The distribution was further modified to obtain a distribution with a mean value of $\overline{f}_4$ and a width of σ_{f_4} (see the Appendix for further explanation).

Once the number of replicas n_r (see Sec. III E), the starting field (h_0), and the acceptance probability between adjacent replicas are fixed, the $\overline{f}_4$ and h_i for replicas ($i=1$ to $n_r -1$) that give us the desired acceptance probability can be obtained by solving iteratively starting from the h_0. A set of 50 000 random numbers were generated initially that corresponds to a mean value of $\overline{f}_4$ (h_0) and a width of distribution σ_{f_4} (h_0). Later, a different set of random numbers were generated that corresponds to a distribution with a mean value of $\overline{f}_4$ (h) and a width of distribution σ_{f_4} (h), where $h < h_0$. The random numbers are then selected sequentially from the two bins and MC moves are attempted. The acceptance probability was determined using Eq. (12). This procedure was repeated by changing h $(< h_0)$ until the desired acceptance probability was achieved. Once the value of h_1 was achieved (the converged value of h), the procedure was repeated for the rest of the fields h_i. The characteristic values of σ_{f_4} and τ_{terminal} at the fields h_i are then interpolated from the values obtained from short serial simulations in $NVTh$ ensemble and their dependencies on $\overline{f}_4$.

The fluctuations observed in f_4 at each field by employing a typical Gaussian random number generator will follow the Gaussian white-noise statistics, i.e., successive values of f_4 are not correlated. However, the fluctuations in f_4 (or any other thermodynamic quantity) of a real system in $NVTh$ ensemble are correlated in time and a characteristic time is often involved in such correlations. In order to reflect the fluctuations of real system in time, it is essential to incorporate a random number generator that accommodates these correlations. Therefore, we have employed a correlated random number generator based on exact time domain method by Percival (See the Appendix for formulation).[44] In this methodology, the time correlations can be incorporated using a predefined correlation sequence ($s_{t,y}$ in the Appendix). These correlated random numbers are also essential in capturing the effect of replica exchange attempt frequency on the efficiency of the algorithm. The correlation sequence ($s_{t,y}$) in formulation can then be directly obtained from the autocorrelation function of f_4 from short serial simulations in $NVTh$ ensemble averaged over statistics from simulations at discrete fields. The autocorrelation function of ghost fraction is given by

$$A(t) = \frac{\langle [f_4(t_0 + t) - \overline{f}_4][f_4(t_0) - \overline{f}_4] \rangle}{\langle [f_4(t_0) - \overline{f}_4][f_4(t_0) - \overline{f}_4] \rangle}. \tag{14}$$

C. Model PST simulations

Once the fields h_i for a particular set of tempering conditions (number of replicas/fields, the acceptance probability, and the exchange frequency) are known, a Gaussian random number corresponding to the distributions at each field was obtained. An exchange of configuration between adjacent replicas was then attempted mimicking the actual parallel tempering simulation following Eq. (12). The procedure was repeated and after every failed attempt of exchange of neighboring replicas, a new random number that was correlated with the previous random number (see Sec. IV B to obtain correlated random number sequence) was used for the next attempt to exchange the same replicas. Once the replicas are exchanged, they acquire new fields and the random number generation corresponding to these distributions in f_4 have been reinitialized (the random number obtained for the next attempt was not correlated with the previous random number since the replicas were exchanged and simulated at a new field). This procedure was repeated until 100 decorrelated structures have been obtained. In case of model PST runs, the decorrelation in structure in a replica was measured by the time spent by that replica in each field. Each field is associated with a relaxation time τ_{terminal} and the total decorrelation of structure in a replica is the sum of decorrelation achieved at each field (based on the time spent at that field and the corresponding relaxation time). It is important to note that the statistics (total relaxation times) were only collected when a replica visits the field h_0 (the equilibrium structure at this field represents that of the unperturbed system). It is possible that a replica can undergo more than one relaxation before it revisits the field h_0 depending upon the time spent at every other field.

Several independent sets of model PST runs are performed by changing the initial seed that generates the correlated random sequence to obtain the normal distribution of f_4 at each field. Statistics are collected and averaged over 100 such independent sets at a particular set of algorithmic conditions $[n_r, P(h_i \Leftrightarrow h_{i+i})$ and the $\omega]$. The efficiency of the PST algorithm (CPU_{MD}/CPU_{PT}) at a particular set of conditions is defined as the ratio of total CPU time (sum of CPU on all nodes/replicas employed) required by PST technique to the CPU time required using conventional MD simulations. The efficiency varies with the number of decorrelated structures obtained. Therefore, it is essential to plot the efficiency of the algorithm as a function of number of independent decorrelated structures obtained.

Thus the model PST runs can be performed at different values of $P(h_i \Leftrightarrow h_{i+i})$, ω, and n_r. The efficiency of the algorithm was calculated by averaging over 100 independent runs at each set of tempering parameters and the optimal values for parameters were obtained.
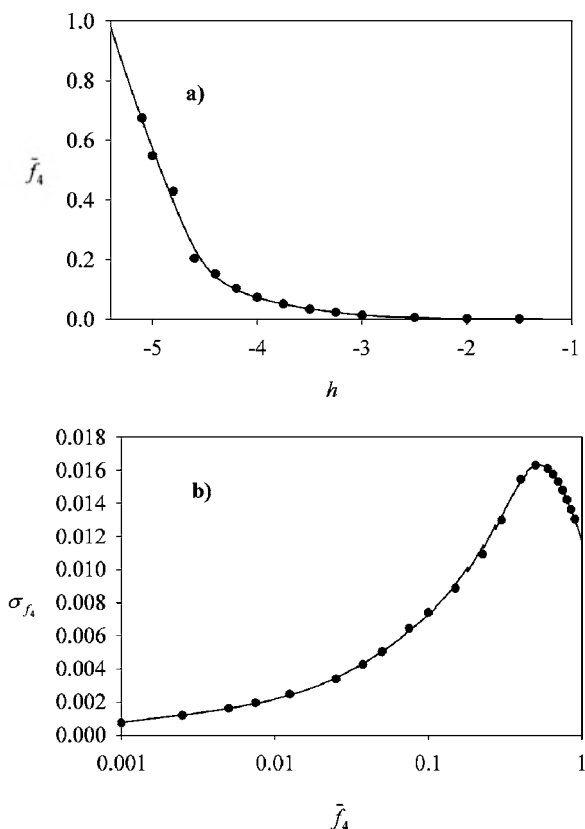
FIG. 7. Characteristic curves obtained from serial *NVTh* simulations at T =0.1. (a) Average fraction of ghost particles ($\bar{f}_4$) as a function of external field (h). (b) The width of the distribution (σ_{f_4}) of fraction of ghost particles as a function of average fraction of ghost particles ($\bar{f}_4$).

V. APPLICATION OF PARALLEL SELECTIVE TEMPERING TO SELF-ASSOCIATING POLYMER SOLUTIONS

A. Optimization of tempering parameters

1. Serial runs

It is evident that the interactions responsible for self-association will be relaxation limiting. Hence an obvious choice for tempering would be these interactions (between end groups and other particles). Sticky end groups comprise 25% (2000 particles) of the total particles in the system. These end groups were allowed to move from real space to ghost space and vice versa. Serial simulations (no exchange) were performed in *NVTh* ensemble at various fields at T =0.1 for 2×10^6 steps with time step 0.01. Based on these short runs, $\bar{f}_4(h)$, $\sigma_{f_4}(\bar{f}_4)$, and $\tau_{\text{terminal}}(\bar{f}_4)$ were obtained (see procedure in Sec. IV A). Figure 7(a) illustrates the effect of field on $\bar{f}_4$ at T=0.1. In Fig. 7(b), σ_{f_4} is plotted against $\bar{f}_4$. The width of the distribution increases as $\bar{f}_4$ increases until it reaches a maximum value and then decreases as $\bar{f}_4 \to 1$. The information obtained from Fig. 7 along with Fig. 4(a) was fed into the statistical model described in Sec. IV. The starting field h_0 was chosen such that $\bar{f}_4$=0.001. This very conservative choice of h_0 means that equilibrium statistics will be collected for configurations that have on average only 2 (0.001 × 2000) ghost particles. The influence of h_0 on the efficiency of PST is discussed later in Sec. VI A. The auto-

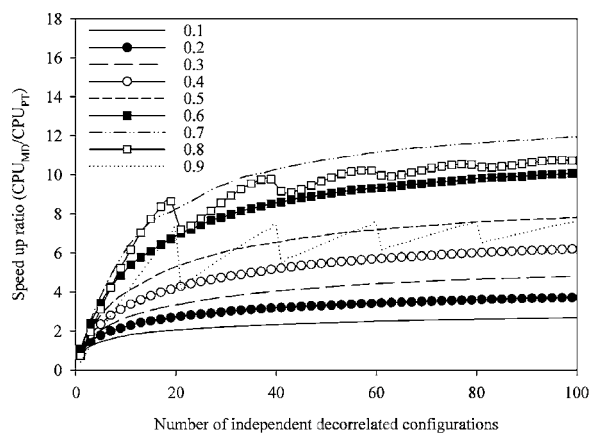correlation function of ghost fraction, given by Eq. (14), was calculated from the fluctuations of f_4 in serial runs in *NVTh* ensemble. At T=0.1, the correlation time calculated by fitting Eq. (14) to the stretched exponential and integrating over time was found to be 889. The correlation time thus obtained was averaged over statistics obtained from *NVTh* simulations at discrete values of h.

2. Model PST runs

Model PST runs were then performed for various number of replicas (2–200), acceptance probabilities (0.1–0.9 with intervals of 0.1) and the replica exchange attempt frequency (0.0008–0.4) between neighboring replicas. The model PST runs were carried out until we obtained 100 independent decorrelated configurations (defined earlier in Sec. IV B). Typically 100 runs were performed (using independent initial seed for correlated random number generator) for each set of tempering parameters in order to obtain good statistics and error bars.

The model PST runs revealed that the efficiency of the algorithm varies significantly with the probability of acceptance of switching configurations between neighboring replicas (keeping a constant number of replicas). Figure 8 shows the effect of acceptance probability on the efficiency of the algorithm. The efficiency is shown as a function of acceptance probabilities ranging from 0.1 to 0.9 for a chain of 20 replicas/fields and an exchange frequency of 0.008. It is obvious from the figure that the PST scheme is inefficient if the objective is to obtain only a few equilibrium structures. However, the speedup ratio (see Sec. IV C) increases as the required number of decorrelated system configurations obtained increases. An optimal acceptance probability for replica exchange is 0.7 for our chosen criteria of 100 decorrelated configurations from 20 replicas.

The efficiency of the PST algorithm as a function of number of replicas simulated (model PST runs) at respective optimum acceptance probability is shown in Fig. 9(a). It is clear that there is a range of number of replicas that can give approximately the same computational efficiency. Another factor to be considered is the total wall clock time required to
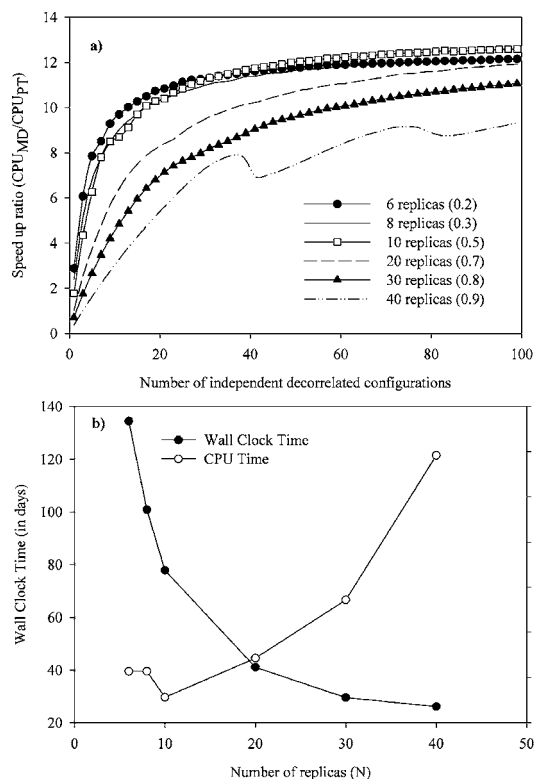
FIG. 9. (a) Efficiency of PST predicted by statistical model for various replicas (6–40) at their optimal acceptance probabilities. (b) The wall clock and CPU time required (in days) to obtain 100 decorrelated configurations as the function of number of replicas. The CPU time=wall clock time × number of replicas.

achieve the goal (e.g., 100 independent decorrelated configurations). Figure 9(b) illustrates the number of CPU and wall clock days required to obtain 100 independent configurations using 20 replicas. The numbers were based on AMD Athlon XP 2200+ (~1800 MHz) CPU. CPU time is just the product of wall clock time and number of replicas. The CPU time has a shallow minimum at 10 replicas consistent with the speedup ratios shown in Fig. 9(a).

We also explored the effect of the replica exchange attempt frequency on the efficiency by performing model PST runs for 20 replicas at optimum acceptance probability (0.7). Figure 10(a) illustrates the effect of exchange frequency on the speedup factor. As seen from the figure, the efficiency is very sensitive to the exchange frequency. In Fig. 10(b), we notice that the optimal value for exchange frequency is about 0.08 for 20 replicas.

B. Validation of statistical model

In order to validate the statistical model we performed the actual PST simulation at $T=0.1$ using 20 replicas at acceptance probability of 0.6 between the neighboring replicas. Attempts to swap the neighboring replicas were made after every 0.008. The starting field (h_0) corresponds to a value that corresponds to $\bar{f}_4=0.001$ whereas the last field (h_{19}) corresponds to $\bar{f}_4=0.036$. In Fig. 6 the acceptance probabilities between adjacent replicas in actual PST simulation are compared to the predicted values for the PST statistical model. The efficiency (speedup ratio) of the actual PST method is
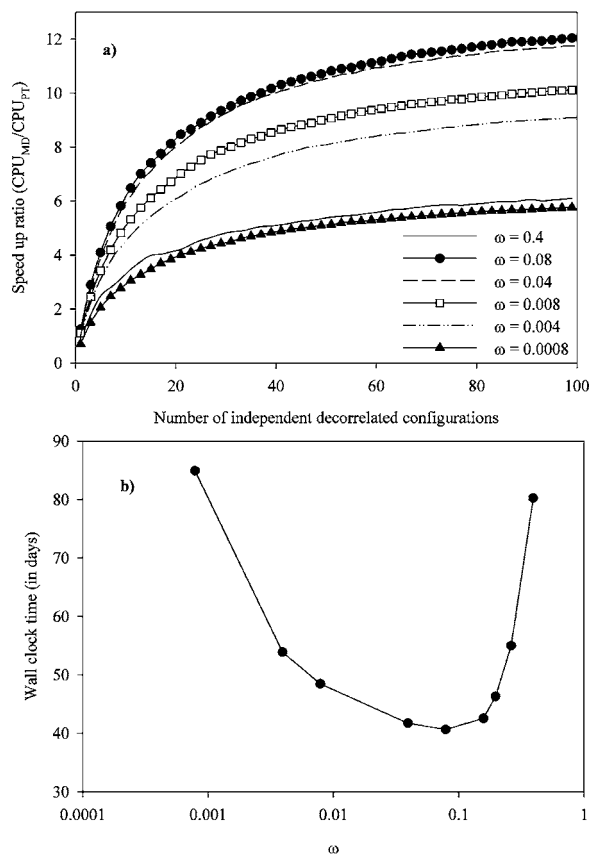

FIG. 10. (a) Efficiency of PST predicted by statistical model as a function of replica exchange attempt frequency (b) wall clock time required in days as the function of replica exchange attempt frequency for 20 replicas with 0.6 acceptance probability.

compared to the predictions made by the model PST simulations in Fig. 11. As seen from Figs. 6 and 11, excellent agreement between the model PST simulation and the actual PST simulation is obtained.

VI. EFFICIENCY OF PARALLEL SELECTIVE TEMPERING METHOD

The end-group cluster size distribution at $T=0.1$ calculated after 75 decorrelated configurations obtained from PST simulations is illustrated in Fig. 12. Also shown for compari-
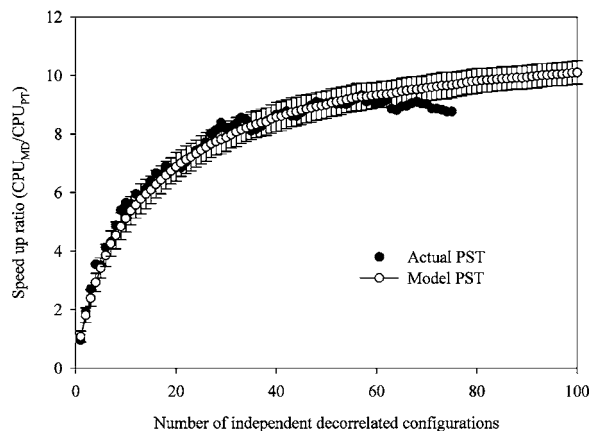

FIG. 11. Efficiency of actual PST simulation and model PST simulation for $n_r=20$, $\omega=0.008$, $T=0.1$, and acceptance probability=0.6.
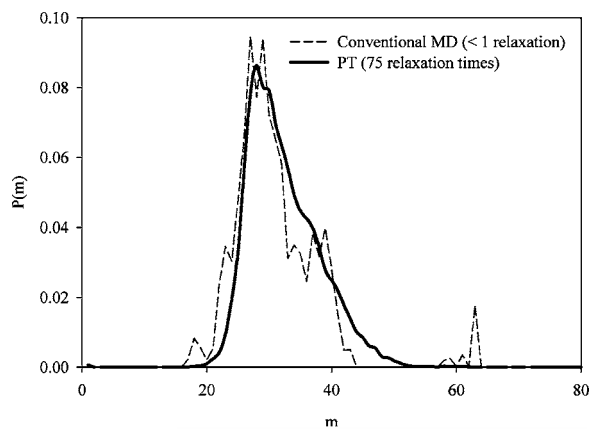
FIG. 12. Cluster size distribution of self-associating polymer solutions at $T=0.1$ from conventional MD and actual PST simulations.
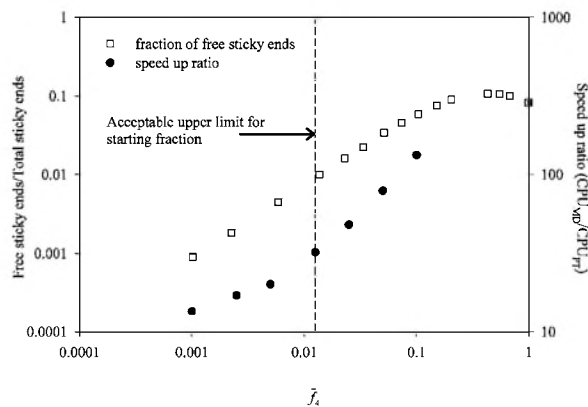

FIG. 13. Clusters of size 1 (free end groups) of self-associating solutions at $T=0.1$ for various values of average starting tempering fraction $[\bar{f}_4(h_0)]$. Also shown are the corresponding efficiencies of PST at these fractions.

son is the cluster size distribution obtained from a conventional *NVT* MD simulation at the same temperature. The wall clock time for the conventional MD simulation, which yields a trajectory that is shorter than the structural relaxation time at this temperature, corresponds to that of the PST simulation. We observe a dramatic improvement in statistics from the PST simulation. Most notable is the disappearance of large clusters ($m \sim 60$) that are apparently an artifact of the nonequilibrium sampling in the conventional MD simulation.

It is clear that the PST algorithm greatly accelerates the generation of equilibrium configurations of the self-associating polymer solution compared to conventional MD simulation. In the case of self-associating dilute solutions at $T=0.1$, the algorithm is at least an order of magnitude faster than the conventional MD simulation. The speedup depends upon the thermodynamic conditions, size of the system, and algorithmic parameters such as number of replicas, replica exchange attempt frequency, and the fields. Optimization of the number of replicas, replica exchange attempt frequency, and the fields has been discussed in Sec. IV. Here we investigate the role of starting field, system size effects, and compare PST with conventional temperature parallel tempering.

A. Choice of starting field

As the particles move from real space to nonphysical space, the structure is perturbed. The extent of this perturbation needs to be clearly understood in order to fix the starting field for PST simulations. Since the particles that are tempered are the sticky groups that form clusters, these sticky groups in ghost space are free to move in the interstitial regions between clusters. Once they make their transition into real space (when all the interactions are turned on), they attach to another cluster. This mechanism of hopping of particle from one cluster to another is responsible for accelerated structural relaxation obtained with PST. It is evident from this process that the perturbation in structure due to the particles in ghost space can be measured by calculating the distribution of free sticky groups (clusters of size 1 in cluster size distribution). In Fig. 13, the number of free sticky groups normalized by total number of sticky ends is plotted against the average fraction of ghost particles. At $\bar{f}_4=0.001$,

corresponding to the h_0 used in the PST simulation discussed above, the fraction of free sticky ends was about 0.0008 indicating that the influence of tempering on structure was minimal. Basing the choice of starting fraction $\bar{f}_4(h_0)$ on the fraction of free sticky ends as shown in Fig. 13, we determined that an upper limit of $\bar{f}_4(h_0)=0.0125$ (this value corresponds to the fraction of free sticky ends to be 0.01) to be reasonable after comparing the radial distribution function for the end groups obtained at this value to that for the untempered system.

The efficiency of PST as defined earlier is also shown in Fig. 13 as a function of $\bar{f}_4(h_0)$ as obtained from model PST simulations. Based on the definition of efficiency in our case (CPU_{MD}/CPU_{PT}), we can see that the efficiency of the PST method depends upon $\bar{f}_4(h_0)$. This increase in efficiency is due to the intrinsic speedup of dynamics at field h_0 (seen by the reduction of $\tau_{terminal}$ at h_0 as we decrease h_0 further). For $\bar{f}_4(h_0)=0.0125$, the maximum acceptable value, model calculations show the PST method to be 2.5 times more efficient than for the more conservative $\bar{f}_4(h_0)=0.001$.

B. Influence of temperature

The effect of temperature on the efficiency of the PST algorithm was observed by simulating self-associating solutions at various temperatures using the statistical model. In addition to simulations at $T=0.1$, we performed simulations at $T=0.13$ and $T=0.07$. In order to utilize the statistical model at $T=0.13$, the input parameters to the model have been evaluated at that temperature. Short serial runs were also performed at $T=0.13$ to investigate characteristic dependencies, $\bar{f}_4(h)$, $\sigma_{f_4}(\bar{f}_4)$, and $\tau_{terminal}(\bar{f}_4)$ of the system. The starting field h_0 was chosen to obtain a corresponding $\bar{f}_4(h_0)=0.001$ similar to the investigations at $T=0.1$. Optimal parameters and the highest efficiency at that temperature are obtained subsequently by performing the model PST runs under different algorithmic conditions. However, as we lower the temperature, obtaining input parameters for the statistical model becomes computationally unachievable due to the exponential increase in relaxation times. Therefore, in order to simulate using the statistical model at $T=0.07$, ex-

trapolation techniques were employed. The characteristic dependencies are extrapolated based on the values at higher temperatures. Later, the model PST runs were performed and the optimal algorithmic parameters that give us the highest efficiency are noted. The efficiency of PST at different temperatures is plotted in Fig. 3 in terms of apparent relaxation times. The apparent relaxation time at any particular temperature is defined as the chain end-to-end vector relaxation time observed in MD simulation at that temperature times the speedup observed due to the algorithm. The apparent relaxation times from PST deviate increasingly from the Arrhenius behavior seen from *NVT* MD simulations as we approach lower temperatures, indicating that the algorithm is more efficient at low temperatures. Specifically, the algorithm at $T=0.07$ is 150 times more efficient than at $T=0.1$ and about 1500 times more efficient than at $T=0.13$.

C. Size effects

The width of the distribution of any thermodynamic quantity such as energy scales as $N^{-1/2}$, whereas the average scales as N (N refers to system size). This poses a particular problem for parallel tempering methods that rely on the overlap of distributions of energies between adjacent replicas/fields in that as the system size increases the number of replicas required to obtain reasonable overlap increases. In order to investigate the effect of N on PST efficiency we have performed model PST runs on various system sizes. The characteristic dependencies of the system are obtained in the following manner. Similar to any other thermodynamic quantity, the normalized width (actual width normalized by the system size) of the distribution in f_4 scales as $N_{\text{allowable}}^{-1/2}$ [see Eqs. (10) and (13)]. Therefore,

$$\sigma'_{f_4}(\bar{f}_4, N'_{\text{allowable}}, T) = \sigma_{f_4}(\bar{f}_4, N_{\text{allowable}}, T)\left(\frac{N'_{\text{allowable}}}{N_{\text{allowable}}}\right)^{-1/2},$$

(15)

where $N'_{\text{allowable}}$ is the size of the new system. Note that $\bar{f}_4(h)$ and $\tau_{\text{terminal}}(\bar{f}_4)$, are independent of system size. The dependencies (based on the new system size) are later fed into the model and the highest efficiency is obtained at optimal parameters from the model.

The speedup obtained from model PST runs as a function of system size at $T=0.1$ is illustrated in Fig. 14. All system sizes are normalized by the base system of 2000 allowable particles. As we increase the size of the system, we observe that the efficiency of PST is decreased. However, due to intrinsically larger speedup obtained in PST, one can extend the limit of simulated system size farther, particularly at lower $T(0.07)$.

D. Comparison with temperature parallel temperature (TPT)

Results obtained from PST are compared to another form of parallel tempering algorithm, namely, TPT where the controlling parameter is the temperature. Various replicas are simulated under similar conditions (N, V) but differing in temperature (T). In order to investigate the efficiency of TPT,
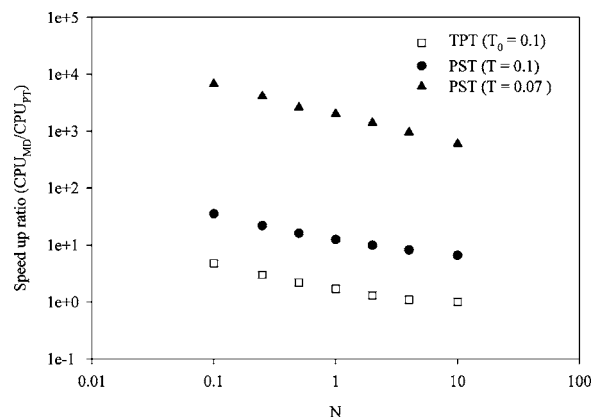

FIG. 14. Efficiency of PST and temperature parallel tempering (TPT) as a function of system size. The abscissa is normalized by the number of sticky ends and T_0 is the temperature of the first replica in TPT.

model TPT runs were performed at various temperatures. It is important to observe that the characteristic dependencies that are required for the statistical model differ from the PST algorithm. Specifically, the important dependencies in TPT are

$$V = V(T, N),$$

$$\sigma_v = \sigma_v(T, N) = [K_b T^2 C_v]^{1/2},$$

$$\tau^T_{\text{terminal}} = \tau^T_{\text{terminal}}(T),$$

(16)

where V is the potential energy of the system in *NVT* ensemble, τ^T_{terminal} is the terminal relaxation time at temperature T and σ_v is the standard deviation in fluctuations in potential energy, and N is the system size. These characteristic dependencies of the system are obtained from MD simulations at various temperatures. The relaxation times from MD simulations were obtained by calculating chain end-to-end vector autocorrelation function and subsequently fitting to stretched exponential and integrating over time [see Eq. (4)]. To obtain the efficiency of TPT at each temperature, model TPT runs were performed at optimal algorithmic parameters. The parameters that influence the efficiency of TPT are the starting temperature (T_0), the number of replicas, replica exchange acceptance probability, and the exchange frequency. Optimal parameters are chosen by investigating the efficiency (defined in Sec. IV) for various conditions. At each set of algorithm conditions, 100 independent sets of model TPT runs were performed and the statistics were collected until we obtain 100 independent decorrelated configurations (similar to investigations performed with PST algorithm at $T=0.1$). Apparent relaxation times, defined in Sec. VI B, as a function of temperature for TPT are also shown in Fig. 3. It is evident from the figure that the TPT performs better than the conventional MD simulation. However, it is inferior to PST (as seen from the figure) and the advantage of PST over TPT is significantly enhanced at lower temperatures. In our comparison of efficiency between PST and TPT, we did not take into account the ability of the TPT method to provide statistics for all temperatures used in the chain of replicas.

124912-12   Ayyagari, Bedrov, and Smith

J. Chem. Phys. **123**, 124912 (2005)

We further compared the efficiency of TPT to PST as a function of system size. Model TPT runs were performed at different system sizes by changing the characteristic dependencies. Specifically,

$$V' = VN'/N,$$

$$\sigma_v(T,N') = \sigma_v(T,N) * (N'/N)^{-1/2}, \tag{17}$$

where V' is the potential energy of system with N' particles. The efficiency thus obtained at various system sizes (normalized by the base system) is compared to the efficiency of PST (see Fig. 14). We observe that as we increase the system size, it becomes more efficient to decouple the trajectories in TPT and run independent configurations (corresponds to ratio $CPU_{MD}/CPU_{PT}=1$).

Based on the investigations made on self-associating solutions, it is evident that this novel parallel selective tempering algorithm can be effectively used to reduce the time required to obtain equilibrium configurations of complex systems. The algorithm has an edge over the current temperature parallel tempering approach. With the aid of the statistical model developed, the algorithmic parameters can be tuned to maximize the efficiency.

VII. CONCLUSIONS

We have developed and implemented a new parallel tempering algorithm based on tempering a fraction of interactions responsible for slowing down the dynamics in the system. Structural relaxation times are related to the fraction of tempered particles (or interactions associated with them), the higher the fraction, the smaller the relaxation time. A chain of independent replicas is then simulated under the extended (*NVTh*) ensemble. Occasionally, the adjacent replicas are swapped by employing the Metropolis rule. Acceptance probability of swapping is dependent upon the extent of overlap of energy distributions of replicas. Thus, in order for the algorithm to be efficient, the choice of various parameters (number of replicas, external fields associated with the replicas, and the swapping frequency between the replicas) has to be optimized. We have developed a statistical model to identify the effects of these parameters on the efficiency of the algorithm and choose the optimal values.

We employed this novel algorithm for simulating self-associating polymer solutions and compared to MD simulation and other parallel tempering (TPT) methods. The algorithm performs better compared with conventional temperature parallel tempering at lower temperatures. There was a significant increase in the dynamics of the system by tempering only a fraction of interactions in contrast with TPT where the system needs to visit high temperatures to obtain a similar increase in dynamics. Thus, PST performs better at lower temperatures (the temperatures of interest). Also, due to the intrinsic efficiency of PST, even though the scaling behavior of PST is similar to any other parallel tempering methodologies, one can extend the limits of system size. This algorithm gives us a substantial improvement over TPT on large systems.

ACKNOWLEDGMENTS

The authors would like to acknowledge the support from Center for Simulations of Accidental Fires and Explosions (C-SAFE) funded by Department of Energy, Lawrence Livermore National Laboratory, under Subcontract No. B524196 and National Science Foundation Grant No. ITR: CHE0312226.

APPENDIX: GENERATING CORRELATED RANDOM NUMBERS WITH EXACT TIME DOMAIN METHOD

Let $W_0, \ldots, W_{N-1}$ be a set of N independent Gaussian random numbers with zero mean and unit variance. With $Y_0 = \sigma_0 W_0$, we generate $N-1$ remaining correlated samples recursively via the following equations:

$$Y_t = \sum_{j=1}^{t} \phi_{j,t} Y_{t-j} + W_t \sigma_t, t = 1, \ldots, N-1.$$

The σ_t's and $\varphi_{j,t}$ are obtained by setting $\sigma_0^2 = s_{0,Y}$ and recursively computing for $t = 1, \ldots, N-1$ by

$$\phi_{t,t} = \frac{s_{t,Y} - \sum_{j=1}^{t-1} \phi_{j,t-1} s_{t-j,Y}}{\sigma_{t-1}^2},$$

$$\phi_{j,t} = \phi_{j,t-1} - \phi_{t,t} \phi_{t-j,t-1}, 1 \leq j \leq t-1,$$

$$\sigma_t^2 = \sigma_{t-1}^2 (1 - \phi_{t,t}^2),$$

where $s_{t,Y}$ is the predefined autocorrelation sequence. The correlated samples Y_t's obtained by the above equations have zero mean and unit variance. They can further be modified to obtain the random numbers with an average $\langle N \rangle$ and variance S by

$$Y_t = Y_t * S + \langle N \rangle.$$

[1] B. Berg and T. Neuhaus, Phys. Lett. B **267**, 249 (1991).
[2] B. Berg and T. Neuhaus, Phys. Rev. Lett. **68**, 9 (1992).
[3] B. Hessebo and R. B. Stinchcombe, Phys. Rev. Lett. **74**, 2151 (1995).
[4] D. D. Frantz, D. L. Freeman, and J. D. Doll, J. Chem. Phys. **93**, 2769 (1990).
[5] W. Ortiz, A. Perlloni, and G. E. Lopez, Chem. Phys. Lett. **298**, 66 (1998).
[6] F. A. Escobedo and J. J. de Pablo, J. Chem. Phys. **105**, 4391 (1996).
[7] A. P. Lyubartsev, A. A. Martinovski, S. V. Shevkunov, and P. N. Vorontsov-Velyaminov, J. Chem. Phys. **96**, 1776 (1992).
[8] E. Marinari and G. Parisi, Europhys. Lett. **19**, 451 (1992).
[9] F. Calvo and J. P. K. Doye, Phys. Rev. E **63**, 010902 (2000).
[10] M. C. Tesi, E. J. Janse van Rensburg, E. Orlandini, and S. G. Whittington, J. Stat. Phys. **82**, 155 (1996).
[11] U. H. E. Hansmann, Chem. Phys. Lett. **281**, 140 (1997).
[12] M. G. Wu and M. W. Deem, Mol. Phys. **97**, 559 (1999).
[13] R. Faller and J. J. de Pablo, J. Chem. Phys. **116**, 5419 (2002).
[14] Q. Yan and J. J. de Pablo, J. Chem. Phys. **113**, 1 (2000).
[15] A. Mitsutake, Y. Sugita, and Y. Okamoto, J. Chem. Phys. **118**, 6664 (2003).
[16] R. Yamamoto and W. Kob, Phys. Rev. E **61**, 5473 (2000).
[17] D. Bedrov and G. D. Smith, J. Chem. Phys. **115**, 1121 (2001).
[18] A. Mitsutake, Y. Sugita, and Y. Okamoto, J. Chem. Phys. **118**, 6676 (2003).
[19] A. Bunker and B. Dunweg, Phys. Rev. E **63**, 016701 (2000).
[20] C. De Michele and F. Sciortino, Phys. Rev. E **65**, 051202 (2002).
[21] B. Joo, B. Pendleton, S. M. Pickles, Z. Sroczynski, A. C. Irving, and J. C. Sexton, Phys. Rev. D **59**, 114501 (1999).

[22] E.-M. Ilgenfritz, W. Kerler, M. Muller-Preussker, and H. Stuben, Phys. Rev. D **65**, 094506 (2002).

[23] S. B. Opps and J. Schofield, Phys. Rev. E **63**, 056701 (2001).

[24] Q. Yan and J. J. de Pablo, J. Chem. Phys. **111**, 9509 (1999).

[25] J. P. Neirotti, F. Calvo, D. L. Freeman, and J. D. Doll, J. Chem. Phys. **112**, 10340 (2000).

[26] F. Calvo, J. P. Neirotti, D. L. Freeman, and J. D. Doll, J. Chem. Phys. **112**, 10350 (2000).

[27] P. Nigra, M. A. Carignano, and S. Kais, J. Chem. Phys. **115**, 2621 (2001).

[28] M. R. Ghayal and E. Curotto, J. Chem. Phys. **113**, 4298 (2000).

[29] J. H. Skone and E. Curotto, J. Chem. Phys. **117**, 7137 (2002).

[30] M. Doxastakis, V. G. Mavrantzas, and D. N. Theodorou, J. Chem. Phys. **115**, 11352 (2001).

[31] K. Makrodimitris, G. K. Papadopoulos, C. Philippopoulos, and D. N. Theodorou, J. Chem. Phys. **117**, 5876 (2002).

[32] I. Andricioaei and J. E. Straub, J. Chem. Phys. **107**, 9117 (1997).

[33] C. Predescu, M. Predescu, and C. V. Ciobanu, J. Chem. Phys. **120**, 4119 (2004).

[34] W. Paul and M. Muller, J. Chem. Phys. **115**, 630 (2001).

[35] D. Bedrov, G. D. Smith, and J. F. Douglas, Europhys. Lett. **59**, 384 (2002).

[36] D. Bedrov, G. Smith, and J. F. Douglas, Polymer **45**, 3961 (2004).

[37] P. G. Khalatur, A. R. Khokhlov, J. N. Kovalenko, and D. A. Mologin, J. Chem. Phys. **110**, 6039 (1999).

[38] J. Ryckaert, G. Cicotti, and H. J. C. Berendsen, J. Comput. Phys. **23**, 327 (1997).

[39] M. P. Allen and D. J. Tildesley, *Computer Simulations of Liquids* (Oxford University Press, Oxford, 1987).

[40] S. Nose, J. Chem. Phys. **81**, 511 (1984).

[41] W. G. Hoover, Phys. Rev. A **31**, 1695 (1985).

[42] D. A. McQuarrie, *Statistical Mechanics* (Harper & Row, New York, 1976).

[43] W. H. Press, S. A. Teukolsky, W. T. Vetterling, and B. P. Flannery, *Numerical Recipes in Fortran 77*, 2nd ed. (Cambridge University Press, Cambridge, 1992).

[44] D. B. Percival, Comput. Sci. Stats. **24**, 534 (1992).